Strong light scattering of highly oxygenated organic aerosols impacts significantly on visibility degradation

Li Liu[1], Ye Kuang[2,3*], Miaomiao Zhai[2,3], Biao Xue[2,3], Yao He[2,3], Jun Tao[2,3], Biao Luo[2,3], Wanyun Xu[4], Jiangchuan Tao[2,3], Changqin Yin[1,7], Fei Li[1,5], Hanbing Xu[6], Tao Deng[1], Xuejiao Deng[1], Haobo Tan[1], Min Shao[2,3]

[1] Institute of Tropical and Marine Meteorology, China Meteorological Administration, Guangzhou, 510640，China

[2] Institute for Environmental and Climate Research, Jinan University, Guangzhou, China.

[3] Guangdong-Hongkong-Macau Joint Laboratory of Collaborative Innovation for Environmental Quality, Guangzhou, China.

[4] State Key Laboratory of Severe Weather & Key Laboratory for Atmospheric Chemistry, Institute of Atmospheric Composition, Chinese Academy of Meteorological Sciences, Beijing, 100081, China

[5] Xiamen Key Laboratory of Straits Meteorology, Xiamen Meteorological Bureau, Xiamen, 361012, China

[6] Experimental Teaching Center, Sun Yat-Sen University, Guangzhou 510275, China

[7] Shanghai Key Laboratory of Meteorology and Health, Shanghai Meteorological Bureau, Shanghai 200030, China

*Correspondence to: Ye Kuang (kuangye@jnu.edu.cn)

Abstract

Secondary organic aerosols (SOA) account for a large fraction of atmospheric aerosol mass and play significant roles in visibility impairment by scattering solar radiation. However, comprehensive evaluations of SOA scattering abilities under ambient relative humidity (RH) conditions on the basis of field measurements are still lacking due to the difficulty of simultaneously direct quantifications of SOA scattering efficiency in dry state and SOA water uptake abilities. In this study, field measurements of aerosol chemical and physical properties were conducted in Guangzhou winter (lasted about three months) using a humidified nephelometer system and aerosol chemical speciation monitor. A modified multilinear regression model was proposed to retrieve dry state mass scattering efficiencies (MSE, defined as scattering coefficient per unit aerosol mass) of aerosol components. The more oxidized oxygenated organic aerosol (MOOA) with O/C ratio of 1.17 was identified as the most efficient light scattering aerosol component. On average, 34% mass contribution of MOOA to total submicron organic aerosol mass contributed 51% of dry state organic aerosol scattering. Overall organic aerosol hygroscopicity parameter κ_{OA} was quantified directly through hygroscopicity closure, and hygroscopicity parameters of SOA components were further retrieved using multilinear regression model by assuming hydrophobic properties of primary organic aerosols. The highest water uptake ability of MOOA among organic aerosol factors was revealed with κ_{MOOA} reaching 0.23, thus further enhanced the fractional contribution of MOOA in ambient organic aerosol scattering. Especially, scattering abilities of MOOA was found to be even higher than that of ammonium nitrate under RH of <70% which was identified as the most efficient inorganic scattering aerosol component, demonstrating that MOOA had the strongest scattering abilities in ambient air (average RH of 57%) during Guangzhou winter. During the observation period, secondary aerosols contributed dominantly to visibility degradation (~70%) with substantial contributions from MOOA (16% on average), demonstrating significant impacts of MOOA on visibility degradations. Findings of this study demonstrate that more attentions need to be paid to SOA property changes in future visibility improvement investigations. Also, more comprehensive studies on MOOA physical properties and chemical formation are needed to better parameterize its radiative effects in models and implement targeted control strategies on MOOA precursors for visibility improvement.

1 Introduction

Atmospheric aerosols directly scatter and absorb solar radiation thus have significant radiative effects on both Earth-Atmosphere radiative budget and atmospheric environment. Aerosols represent the dominant contributor to atmospheric visibility impairment in polluted regions (Liu et al., 2017a). With the rapid industrialization and urbanization, China has been experienced severe haze pollution in recent ten years and frequent low visibility events have aroused public attention and concern, especially since 2013. In recent years, the Chinese government has implemented stringent control policies called "blue sky actions" to lower aerosol mass concentration and improve atmospheric visibility. However, Xu et al. (2020) revealed that the less than expected visibility improvement in southern China, especially the poor visibility improvement in Pearl River Delta region, due to the non-linear responses of visibility improvement to $PM_{2.5}$ (particulate matter with aerodynamic diameter less than 2.5 μm) mass concentration reduction. Several recent literature reports also proved that visibility was less improved than $PM_{2.5}$ mass concentrations. Results of Liu et al. (2020) demonstrated that increased aerosol extinction efficiency associated with nitrate was responsible for the less improved visibility in eastern China. Hu et al. (2021) raised the challenge of visibility improvement due to increased nitrate contribution in Beijing area. However, results of Xu et al. (2020) demonstrate that this situation was likely associated with both increased aerosol scattering efficiency and aerosol hygroscopicity and particularly pointed out that other than changes of inorganic aerosol components, special attention should be paid to scattering efficiency and hygroscopicity changes of secondary organic aerosol (SOA).

Organic aerosols including primary and secondary organic aerosols (POA and SOA) represent a large and sometimes even dominant fraction of submicron aerosol mass (Jimenez et al., 2009). Especially, SOA was found to contribute dominantly to total organic aerosol mass under polluted hazy conditions (Huang et al., 2014;Kuang et al., 2020a). Wang et al. (2019) reported increased contributions of both secondary organic and inorganic aerosol mass across China due to clean air actions, and the nonlinear responses of secondary aerosol mass concentration to emission reductions were further confirmed during COVID lock down period as reported by Huang et al. (2020). Xu et al. (2019) also reported substantial changes of SOA properties such as enhanced oxidation state. However, most previous studies only paid attention to influences of nitrate increase on visibility degradation, whereas synergistic effects of SOA on visibility has never been the focus due to the complexity of

SOA hygroscopicity and scattering efficiency. Organic aerosol evolves in the atmosphere including their sizes and chemical structures thus also their optical properties and hygroscopicity (Jimenez et al., 2009), leading to the difficulty of quantifying contributions of organic aerosol in visibility degradation. Li et al. (2022) reported that nitrate and SOA dominated particle extinction in dry state in Beijing due to clean air actions, however, lacking evaluations in ambient air, stressing further the importance of comprehensive evaluations of SOA scattering abilities under ambient relative humidity (RH) conditions to better elucidate roles of SOA in visibility degradation and long-term visibility changes.

In this study, we comprehensively quantified the dry state mass scattering efficiencies (MSEs) of both primary and secondary organic aerosol components and organic aerosol hygroscopicity, thus systematically evaluated contributions of SOA factors to aerosol scattering and visibility degradation in ambient air.

2 Materials and Methods

2.1 Campaign information

Aerosol physical and chemical properties were simultaneously measured during winter from 13th December 2020 to 25th February 2021 in Guangzhou urban area. Instruments were housed in an air-conditioned container in Haizhu wetland park (Sect.S1 for site information). A $PM_{2.5}$ inlet (BGI, SCC 2.354) was used for aerosol sampling, and sample flow of 8-9 L/min was maintained during the observation period thus generally satisfying the flow requirement (8 L/min) of 2.5 μm cutting diameter. A Nafion drier was used to lower sample RH to less than 40%. A humidified nephelometer system with a total flow of about 5 L/min and a quadrupole-Aerosol Chemical Speciation Monitor Q-ACSM with a flow of 3L/min were placed downstream of the drier to measure aerosol scattering abilities under controlled RH conditions and aerosol chemical compositions. An AE33 aethalometer (Drinovec et al., 2015) set up with a flow rate of 5 L/min was separately operated under another inlet ($PM_{2.5}$, BGI SCC 1.829) to measure aerosol absorptions thus indirectly black carbon (BC) mass concentration. Measurements of meteorological parameters such as temperature, wind speed and direction, and RH were made by an automatic weather station.

2.2 Humidified nephelometer measurements.

The humidified nephelometer system is a laboratory-assembled one, including two Aurora 3000 nephelometers, one measuring aerosol scattering abilities (aerosol scattering and back scattering coefficients at 450, 525 and 635 nm) under low RH conditions (mostly less than 30%, dry

nephelometer) and another one measuring aerosol scattering abilities under controlled RH conditions (wet nephelometer). The humidified nephelometer system can operate either in fixed-RH mode or in scanning RH mode, details about techniques of fixed RH mode and scanning RH mode were introduced in detail in several previous studies (Kuang et al., 2017;Kuang et al., 2020b). In this study, the humidified nephelometer system was operated in scanning RH mode before 26th January 2021 and in fixed RH mode (80% RH) from 26th January to 9th February. The RH ranges of scanning RH mode were 75-90% from 11th December 2020 to 5th January 2021 and 60-90% from 13th to 26th January 2021. The humidified nephelometer system provides direct measurements of aerosol light scattering enhancement factor $f(\mathrm{RH},\lambda) = \frac{\sigma_{sp}(RH,\ \lambda)}{\sigma_{sp}(dry\ \ \lambda)}$ where $\sigma_{sp}(RH,\ \lambda)$ is the aerosol scattering coefficient of light wavelength λ at condition of RH (Titos et al., 2016;Zhao et al., 2019a), and $f(\mathrm{RH}, 525)$ referred directly to as $f(\mathrm{RH})$ was usually used to derive the optical hygroscopicity parameter κ_{sca} through $f(\mathrm{RH}) = 1 + \kappa_{sca} \times \frac{RH}{100-RH}$ (Brock et al., 2016;Kuang et al., 2017;Kuang et al., 2018;Xu et al., 2020;Kuang et al., 2020b;Kuang et al., 2021b). The nephelometer measurements are associated with truncation error and non-ideality of light source. The dry state aerosol scattering coefficients were corrected using the empirical formula provided by Qiu et al. (2021). RH_0 in the dry nephelometer was in the range of 6-49% with an average of 22%, thus dry state aerosol scattering coefficient at 525 nm ($\sigma_{sp,525}$) was further corrected using measured aerosol optical hygroscopicity through $\sigma_{sp,525}=\sigma_{sp,525,measured}/(1+\kappa_{sca} \times \frac{RH_0}{100-RH_0})$.

2.3 Q-ACSM measurements and PMF analysis.

The Q-ACSM was deployed to routinely characterize and measure the mass concentrations of non-refractory submicron aerosol components at a time resolution of 15min, including organics, sulfate, nitrate, ammonium and chloride, details about Q-ACSM set-up please refer to Ng et al. (2011). The mass concentrations and mass spectra were processed using ACSM data analysis software (ACSM Local 1.5.10.0 Released July 6, 2015) based on Igor Pro (version 6.37). The detailed procedures were described in Ng et al. (2011) and Sun et al. (2012). Composition dependent CE value consistent with Middlebrook et al. (2012) and Sun et al. (2013) was chosen considering that aerosol samples was dried before entering the ACSM instrument. According to Middlebrook et al. (2012), CE = max (0.45, 0.0833+0.9167×ANMF), where ANMF is the ammonium nitrate mass fraction in NR-PM1. The results showed that about 10% of samples had CE values larger than 0.45, with the largest value of 0.65. The

average CE value of the samples with a CE greater than 0.45 was 0.5. RIEs of 5.15 and 0.7 from calibration results during the campaign using 300 nm pure ammonium nitrate (AN) and ammonium sulfate (AS) were used for ammonium and sulfate quantifications, while default RIEs of 1.4, 1.1 and 1.3 for organic aerosol, nitrate and chloride were adopted. Positive matrix factorization technique with the multilinear engine (ME-2 (Canonaco et al., 2013;Canonaco et al., 2021)) were used for resolving potential OA factors related with different sources and processes. Four factors were deconvolved, including two primary OA factors and two oxygenated OA factors which were usually treated as SOA. A hydrocarbon-like OA (HOA, O/C~0.15），a cooking-like OA (COA, O/C~0.13), a less oxidized oxygenated OA (LOOA, O/C~0.7), and a more oxidized oxygenated OA (MOOA, O/C~1.17). The mass spectra of these factors (Fig.S9) and more details about the factor analysis could be found in Sect.S2 of the supplement.

2.4 Organic aerosol hygroscopicity derivation.

Organic aerosol was usually treated as nearly hydrophobic in many previous studies when considering environmental effects of organic aerosol (Cheng et al., 2016), however quantified in this study based on the most recently developed organic aerosol hygroscopicity quantification method by Kuang et al. (2019). On the basis of field measurements, organic aerosol hygroscopicity parameter κ (κ_{OA}) can only be estimated through closure between directly measured overall aerosol hygroscopicity and aerosol chemical compositions using the volume mixing rule (Kuang et al., 2020c). Kuang et al. (2020b) developed an optical method to calculate κ_{OA} based on the combination of the humidified nephelometer system measurements and bulk PM_1 aerosol chemical-composition measurements, and the application of this method was further manifested and discussed in Kuang et al. (2021b), thus used in this study to estimate κ_{OA}. The humidified nephelometer system provides direct measurements of the optical hygroscopicity parameter κ_{sca} and aerosol scattering Ångström exponent, which can be used together to derive a κ value referred to as $\kappa_{f(\mathrm{RH})}$ (Kuang et al., 2017) which can be treated as the overall aerosol hygroscopicity parameter in the hygroscopicity closure (Kuang et al., 2021a). In the closure, ions were paired using the scheme proposed by Gysel et al. (2007) as listed in Tab.S1. Same with Kuang et al. (2021b), retrieved $\kappa_{f(\mathrm{RH})}$ at RH of 80% was used as measured average κ of PM1 aerosol populations, κ values of ammonium sulfate (AS) and ammonium nitrate (AN) at 80% RH were predicted using the Extended Aerosol Inorganic Model (E-AIM), and those of ammonium chloride

(AC) and ammonium bisulfate (ABS) were consistent with Liu et al. (2014). Then, the κ_{OA} can be estimated using the following formula by assuming volume additivity and zero κ of BC:

$$\kappa_{OA} = \frac{\kappa_{f(\mathrm{RH})} - (\kappa_{AS}\varepsilon_{AS} + \kappa_{AN}\varepsilon_{AN} + \kappa_{ABS}\varepsilon_{ABS} + \kappa_{AC}\varepsilon_{AC} + \kappa_{X}\varepsilon_{X})}{\varepsilon_{OA}} \quad (1)$$

Where ε represents volume fraction whose calculation needs total aerosol volume concentrations and subscript represents name of an aerosol component. The total PM_1 aerosol volume concentration was calculated using measurements of the dry nephelometer following the machine learning method proposed by Kuang et al. (2018). Organic aerosol density varies over a wide range, and previous studies demonstrate that it is tightly associated with aerosol oxidation state (Kuwata et al., 2012) and higher O/C ratio usually corresponds to higher aerosol density. Following Wu et al. (2016) , densities of primary organic aerosol components (POA) including HOA and COA was assumed as 1 g/cm^3, and density of MOOA was assumed as 1.4 g/cm^3 due to its highly oxygenated feature with O/C of 1.17, however, the density of LOOA was assumed as 1.2 g/cm^3 due to its moderate O/C value of 0.7. In addition, the difference between predicted volume concentration from nephelometer measurements and the total aerosol volume concentrations summed from known aerosol components was attributed to aerosol components unidentified by the mass spectrometer, thus its volume fraction and hygroscopicity were named as ε_X and $\kappa_X$in Eq.1, where κ_X was assumed as 0.05 since the unidentified part are usually metals and dust with low aerosol hygroscopicity. For more comprehensive discussions on κ_{OA} estimations as well as κ_X treatment please refer to Kuang et al. (2021b).

Table 1. Densities (ρ) and hygroscopicity parameters (κ) of inorganic salts

Species	NH_4NO_3 (AN)	NH_4HSO_4 (ABS)	$(NH_4)_2SO_4$ (AS)	NH_4Cl (AC)
ρ (g cm^{-3})	1.72	1.78	1.769	1.528
κ	0.56	0.56	0.56	0.93

Using the ZSR mixing rule, the κ_{OA} derived at RH of 80% can be further expressed as:

$$\kappa_{OA} = \varepsilon_{HOA} \times \kappa_{HOA} + \varepsilon_{COA} \times \kappa_{COA} + \varepsilon_{MOOA} \times \kappa_{MOOA} + \varepsilon_{LOOA} \times \kappa_{LOOA} \quad (2)$$

Where ε represents volume fractions of primary and secondary organic aerosol components in total

organic aerosols. Assuming κ values of HOA and COA as zero, Eq.2 can be simplified as $\kappa_{OA} = \kappa_{MOOA} \times \varepsilon_{MOOA} + \kappa_{LOOA} \times \varepsilon_{LOOA}$. Considering the noisy characteristics of derived κ_{OA} as shown in Fig.4a, this simplified formula was not directly used to fit all derived κ_{OA} values. Instead, average diurnal variations of derived κ_{OA} were firstly acquired and then fitted using $\kappa_{OA} = \kappa_{MOOA} \times \varepsilon_{MOOA} + \kappa_{LOOA} \times \varepsilon_{LOOA}$ with average diurnal volume fractions of MOOA and LOOA (ε_{MOOA} and ε_{LOOA}) in total organic aerosol as inputs, which yields average κ_{MOOA} and κ_{LOOA}.

3 Results and discussions

3.1 Overview of the pollution characteristics during Guangzhou winter.

The timeseries of corrected aerosol scattering coefficients in dry state ($\sigma_{sp,525}$), non-refractory PM_1 (NR_{PM1}) mass concentrations, resolved organic aerosol factors as well as meteorological parameters are shown in Fig.1. Scattering coefficient at 525 nm of aerosols in dry state ($\sigma_{sp,525}$) varied over a wide range of 8 to 688 Mm^{-1} with an average of 118 Mm^{-1}. The average NR_{PM1} is 20 μg/m^3 with the highest NR_{PM1} mass concentrations reached beyond 160 μg/m^3. This suggests for relatively clean conditions compared to aerosol pollution in other polluted regions in China (Zhou et al., 2020), however, severe pollution episodes occurred occasionally. Three haze pollution episodes characterized by relatively high aerosol mass loading and scattering coefficients were observed before February (Gray shaded areas in Fig.1). The evolution and formation of these three episodes were tightly associated with the stagnant meteorological conditions as indicated by the low wind speed (< 2 m/s)

and increasing RH during the last two severe pollution episodes. As shown in Fig.1c, organic aerosol and nitrate contributed dominantly to the increase of aerosol mass, while sulfate remains almost flat or increased slightly during these pollution episodes. For example, for the episode with the worst pollution condition occur, the daily average NR_{PM1} increased from 19 to 143 μg/m^3 from 12th to 16th February with the organic aerosol increased from 9.3 to 69.8 μg/m^3 and nitrate increased from 5.5 to

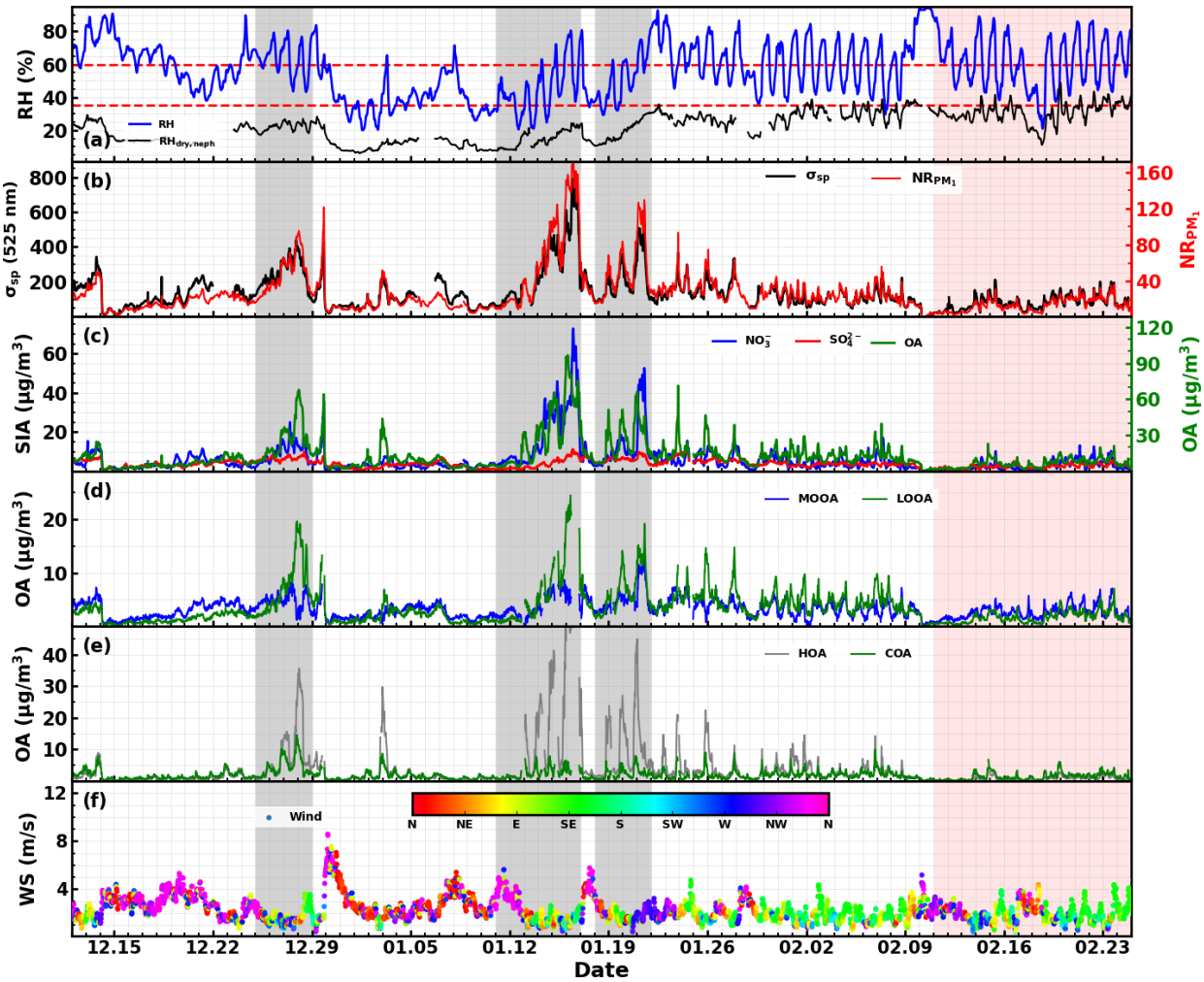

Figure 1. Timeseries of (a) RH; (b) aerosol scattering coefficient in dry state, and NR_{PM1} concentration; (c) Secondary inorganic aerosols (SIA) including sulfate and nitrate, and organic aerosol in right axis, (d) MOOA and LOOA; (e) HOA and COA; (f) wind speed and wind direction. Gray shaded areas are three identified pollution episodes, and pink shaded area is period of spring festival.

44.2 μg/m^3, however, sulfate only increased from 1.4 to 8.5 μg/m^3. This phenomenon is quite different from the results reported by Guo et al. (2020) and Chen et al. (2021b) that organic aerosol dominated the aerosol mass increase with obvious increase of both sulfate and nitrate in pollution episodes in autumn of Guangzhou urban area, however, was generally consistent with the increasing characteristics reported by Chen et al. (2021a). These observations suggest that the aerosol pollution

differs much among seasons and years due to the highly variable characteristics of meteorological conditions. As for the organic aerosol mass increase, the time series of resolved organic aerosol factors are also shown in Fig.1d and Fig.1e. For the three observed pollution episodes, both increases of primary and secondary organic aerosol (represented by summation of MOOA and LOOA) were observed, with LOOA contributing dominantly to SOA increase and HOA contributing dominantly to POA increase. However, the accumulation of POA (summation of HOA and COA) contributed almost twice as much as the increase of SOA, suggesting primary emissions especially vehicle emissions played significant roles in aerosol mass increase during pollution episodes of Guangzhou winter.

3.2 Strong scattering ability of MOOA in dry state.

Traditional multiple linear regression models were usually applied to determine MSEs of different aerosol components using simultaneously measured aerosol scattering coefficients and mass concentrations of aerosol components (Hand and Malm, 2007;Han et al., 2015;Chan et al., 1999). However, the traditional model failed in this study due to co-variations of input variables and impactor inconsistencies ($PM_{2.5}$ versus PM_1) between aerosol chemical compositions and aerosol scattering measurements. Details about this failure was discussed in Sect.S4 of the supplement. A new methodology was proposed to lower correlations between variables and reduce the impacts of measurement inconsistency of aerosol populations between nephelometer and the mass spectrometer. This method considers mainly the responses of aerosol scattering coefficient to quick mass concentration increases of aerosol components. Using AN as an example, obvious increasing cases of AN were identified, average changes of aerosol components as well as $\sigma_{sp,525}$ for these cases are shown in Fig.2a. On average, AN dominated the aerosol mass increase (>90%) in these cases, however, changes of other aerosol components differed much among cases as indicated by large standard deviations. The MSE_{AN} can be roughly estimated as around 7 m^2/g if assuming $\sigma_{sp,525}$ was solely contributed by AN increase. As shown in Fig.1d and Fig.1e, prominent increase of HOA, COA and LOOA were frequently observed. Average changes of aerosol components and $\sigma_{sp,525}$ for identified cases of HOA increase or COA increase are shown in Fig.2b. It shows that increases of HOA or COA were usually accompanied with obvious increases of BC and LOOA, thus the impacts of HOA or COA increases on observed aerosol scattering increases cannot be isolated. Similar results were obtained

with LOOA and MOOA. As shown in Fig.1, remarkable increases of LOOA cases were almost always accompanied with the spontaneously quick HOA increase because most LOOA rapid increase cases

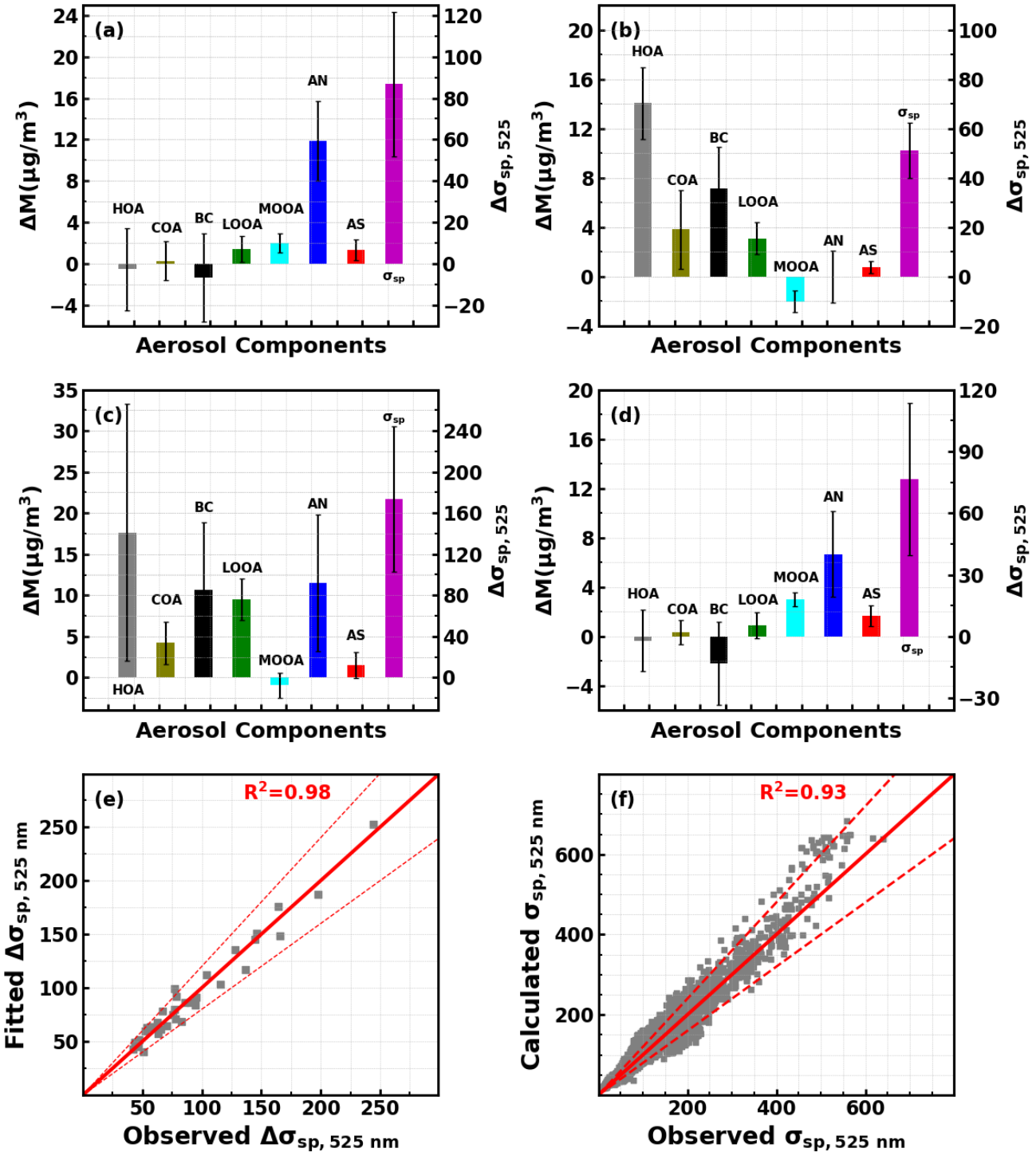

Figure 2. Average changes of aerosol components and $\sigma_{sp,525}$ (right axis) for identified increase cases of (a) Nitrate; (b) HOA; (c) LOOA; (d) MOOA, black error bars represent standard deviations. (e) Comparisons between observed $\sigma_{sp,525}$ changes for identified cases and multiple linear fitted values. (f) The comparison between observed $\sigma_{sp,525}$ and calculated $\sigma_{sp,525}$ using retrieved MSEs of aerosol components. Red dashed lines represent 20% deviation lines.

happened during pollution episodes and start near dusk when accumulation of vehicle emissions and

nitrate formation occurred. Thus, the average increase of LOOA was even smaller than those of AN and HOA. Slight but obvious MOOA increase cases were also identified, and average results are also shown in Fig.2d, showing that MOOA increase were usually accompanied with obvious nitrate formation. These results demonstrate that MSEs of aerosol components cannot be quantified directly from responses of aerosol scattering to aerosol emission or formation processes. However, for these cases, mass increases of aerosol components and corresponding changes in aerosol scattering matter most and impacts of unidentified aerosol components are reduced substantially through differential considering the average time change for these identified cases are only 4 hours. In addition, as listed in Tab.S3, the correlations between changes of most variables for all identified cases are much smaller than their timeseries correlations shown in Tab.S1. Thus, the modified multiple linear regression model $\Delta\sigma_{sp,525} = \Delta HOA \times MSE_{HOA} + \Delta COA \times MSE_{COA} + \Delta LOOA \times MSE_{LOOA} + \Delta MOOA \times MSE_{MOOA} + \Delta AS \times MSE_{AS} + \Delta AN \times MSE_{AN} + \Delta BC \times MSE_{BC}$ was applied to retrieve MSEs of aerosol components. The derived MSEs for HOA, COA, LOOA, MOOA, AN, AS and BC were 2.1, 3.9, 3.4, 9.9, 7.1, 5.5 and 3.3 m^2/g, respectively. The fitted $\Delta\sigma_{sp,525}$ correlated highly (R^2=0.98, average ratio 1.0) with observed $\Delta\sigma_{sp,525}$ as shown in Fig.2e. Derived MSEs were used to calculate $\sigma_{sp,525}$ during the whole observation period using the formula $\sigma_{sp,525} = 2.1 \times HOA + 3.9 \times COA + 3.4 \times LOOA + 9.9 \times MOOA + 5.5 \times AS + 7.1 \times AN + 3.3 \times BC$, and compared with observed $\sigma_{sp,525}$. Good consistency (R^2=0.93 and average ratio of 1.05, Fig.2f) was achieved between calculated and observed $\sigma_{sp,525}$ values. In addition, the retrieved MSE_{AN} (7.1) using the modified multilinear regression model was quite consistent with the estimated one (7 m^2/g) based on average changes shown in Fig.2a, which indirectly confirms the reliability of the modified method.

Tao et al. (2019) quantified MSEs of fine mode AS, AN as well as elemental carbon (EC) using size-resolved filter measurements in four seasons of Guangzhou urban area. Their results demonstrate that MSEs of AN and AS bears relatively large standard deviations and variations among seasons, however, MSE of EC varied little among seasons with small standard deviations (2.6±0.1 m^2/g). The derived MSE_{BC} of 3.3 m^2/g was close to the MSE_{EC} reported in Tao et al. (2019). The derived MSE_{AN} and MSE_{AS} were obviously higher than those reported in previous studies in which MSE_{AN} and MSE_{AS} were estimated through Mie theory of size-resolved filter measurements [Tao et al., 2019;Chen et al., 2020]. For example, Tao et al. (2019) reported MSEs of 4.4±1.3 m^2/g for AN and 4.3±0.9 m^2/g for AS in winter of urban Guangzhou for fine mode aerosols (<2.1 μm). The reason explaining this inconsistency is that

the derived MSE_{AN} using multiple regression method here is $MSE^{*}_{AN} = \frac{\sigma_{sp,525}(AN,PM_{2.5})}{[AN](PM_1)}$, however, MSE_{AN} derived for example in Tao et al. (2019) of fine mode is $MSE_{AN,PM_{2.1}} = \frac{\sigma_{sp,525}(AN,PM_{2.1})}{[AN](PM_{2.1})}$. The $MSE_{AN,PM_{2.1}}$, MSE_{AN,PM_1} and MSE^{*}_{AN} values of 4.4, 5.3 and 7.5 m^2/g are simulated using the reported average AN mass size distributions reconstructed from size-resolved filter measurements in winter of urban Guangzhou by Tao et al. (2019) (as shown in Fig.3a) as inputs of Mie model. The simulated MSE^{*}_{AN} of 7.5 is very close to the retrieved MSE^{*}_{AN} and is much higher than simulated MSE_{AN,PM_1} due to substantial mass contributions of 1 to 2.1 μm as shown in Fig.3a, demonstrating that good consistency between results of the multiple regression model and results of Tao et al. (2019) was achieved.

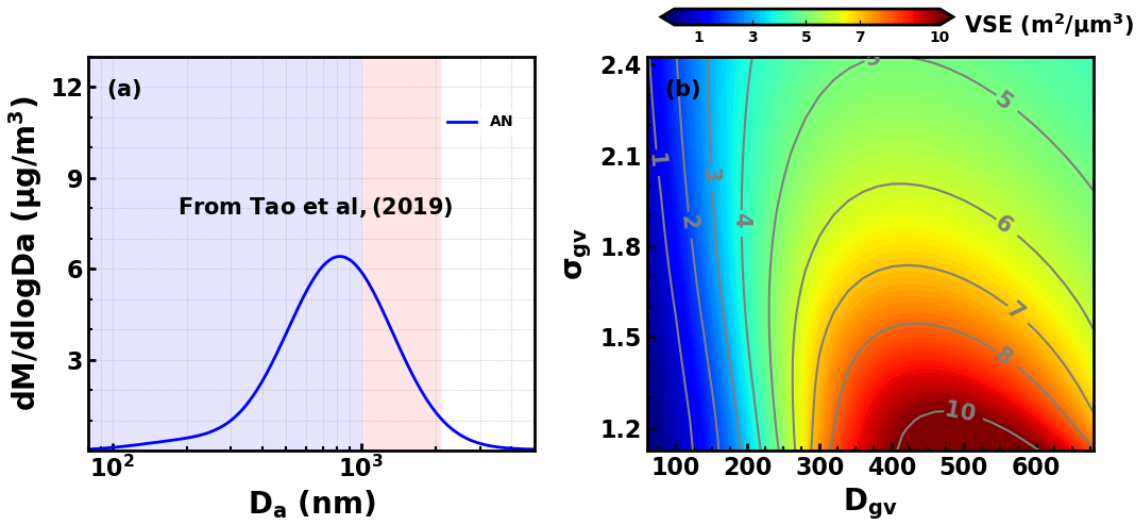

Figure 3. (a) AN mass size distributions derived by Tao et al, (2019) based on size-resolved filter measurements, Da is the aerodynamic diameter; (b) Simulated aerosol volume scattering efficiency (VSE) under different volume size distributions through varying volume geometric mean D_{gv} and standard deviation σ_{gv} of lognormal size distributions. Blue shaded area corresponding to PM_1 and pink shaded area corresponding to $PM_{1\text{-}2.1}$.

If using the simulated ratio $MSE_{AN,PM_1}/MSE^{*}_{AN}$ to approximate MSE_{AN,PM_1}, MSE_{AS,PM_1} and MSE_{MOOA,PM_1}, values of 5.0, 3.9 and 6.9 m^2/g for MSE_{AN,PM_1}, MSE_{AS,PM_1} and MSE_{MOOA,PM_1} would be obtained, which falls in the reported ranges of MSE_{AS} and MSE_{AN} (Tao et al., 2019), however, the high MSE_{MOOA,PM_1} needs further investigation. MSE is determined by the aerosol volume scattering efficiency (VSE) defined as aerosol scattering per unit aerosol volume and aerosol density (ρ_a) with $MSE = \frac{VSE}{\rho_a}$. High MSE^{*}_{MOOA} of 9.9 m^2/g was retrieved, however, most of the difference between MSE^{*}_{MOOA} and MSE^{*}_{AN} might be explained by their density differences. Based on the Mie theory, aerosol scattering is in general proportional to aerosol volume (Kuang et al., 2018), thus the volume

size distribution are determining factors in VSE variations. The VSE of PM_1 under different unimodal volume lognormal distribution conditions with refractive index of $1.53\text{-}10^{-7}i$ were simulated and shown in Fig.3b. The approximated $\mathrm{MSE}_{\mathrm{AN,PM_1}}$ and $\mathrm{MSE}_{\mathrm{MOOA,PM_1}}$ of 5.0 and 6.9 m^2/g corresponds to $\mathrm{VSE}_{\mathrm{AN,PM_1}}$ and $\mathrm{VSE}_{\mathrm{MOOA,PM_1}}$ of 8.6 and 9.7 $\mathrm{m^2/\mu m^3}$ according to the aerosol densities discussed in Sect. 2.4, falling within the VSE ranges of geometric mean diameter (D_{gv}) near 500 nm and geometric standard deviation (σ_{gv}) of 1.3 to 1.5. This result is consistent with conclusions of several previous studies that the MOOA with highest oxygen state that have experienced complex chemical aging such as aqueous phase reactions likely share similar shape of mass/volume size distribution with inorganic secondary aerosols (Kuang et al., 2020a;Wang et al., 2021), and this result rationalizes that using $\mathrm{MSE}_{\mathrm{AN,PM_1}}/\mathrm{MSE}^*_{\mathrm{AN}}$ ratio to derive $\mathrm{MSE}_{\mathrm{AS,PM_1}}$ and $\mathrm{MSE}_{\mathrm{MOOA,PM_1}}$. In addition, aerosol refractive index also played significant roles in aerosol VSE variations (Zhao et al., 2019b;Liu et al., 2013), and the high MSE of MOOA might also be related with the high real part of its refractive index. Laboratory results of Li et al. (2017) revealed enhanced light scattering of SOA formed through multiphase reactions due to increase of the real part of the refractive index. Zhao et al. (2021) reported that real part of aerosol refractive index varied over a wide range (1.36 to 1.78), and in general increased with the mass fraction increase of organic aerosol, suggesting generally higher real part of refractive index of organic aerosol. In general, these results revealed strong scattering abilities of MOOA under dry state, however the size distribution and refractive index of MOOA needs further comprehensive investigations.

Moreover, effective densities of HOA, COA, LOOA are near 1 g/cm^3, suggesting that VSEs of HOA, COA, LOOA are around or slightly higher than their corresponding MSEs. As shown in Fig.3b, $\mathrm{VSE}_{\mathrm{PM_1}} < 4\ \mathrm{m^2/\mu m^3}$ means that D_{gv} was generally lower than 250 nm, thus more than 99% of aerosol mass resided in PM_1 under σ_{gv}<1.8. Therefore, derived MSEs of HOA, COA, LOOA can be treated as their corresponding $\mathrm{MSE}_{\mathrm{PM_1}}$ values. Cai et al. (2020) reported average HOA and COA volume size distributions in urban Beijing using PMF techniques. They found (Fig.7 in Cai et al. (2020)) that HOA volume peaked near 200 nm, and COA volume size distribution showed bimodal characteristics with the first mode peaking near 90 nm and the second mode peaking near 350 nm, yielding MSEs that share similar magnitude with the retrieved MSEs of HOA and COA. These results further confirmed the reliability of the newly proposed multiple regression method.

3.3 Water uptake abilities of organic aerosols

Timeseries of derived κ_{OA} is shown in Fig.4a, estimated κ_{OA} ranged from -0.08 to near 0.35 with an average of 0.09 which is in general consistent with those reported in other regions (Kuang et al., 2020c). It was found that variations of derived κ_{OA} correlated tightly with mass fractions of MOOA (R=0.6) and POA (R=-0.52) as shown in Fig.4b and Fig.4c. The MOOA enhanced the overall κ_{OA} and POA lowered κ_{OA}, which is consistent with conclusions of previous studies, however, no correlations were found between κ_{OA} and mass fractions of LOOA (R=0.06). As shown in Fig.4d and Fig.4e, drastic increase of POA before dusk would bring drastic decrease of κ_{OA} to around 0.05, which are in accordance with reported results in previous literature that most POA components are hydrophobic with κ of almost zero. As introduced in Sect 2.4, the average diurnal variations of volume fractions of MOOA and LOOA were used as variables to fit average diurnal variations of derived κ_{OA} shown in Fig.4e to retrieve κ_{MOOA} and κ_{LOOA}. The fitted results are shown in Fig.4e (R^2=0.89, average ratio of 1), yielding κ_{MOOA} and κ_{LOOA} values of 0.23 and 0.13. The relatively lower value of κ_{LOOA} and sometimes co-increase phenomena of LOOA and POA during dusk period (as shown in Fig.1 and Fig.3d) explain the weak correlations between κ_{OA} and LOOA mass fraction. Most previous field-based organic aerosol hygroscopicity studies focused only on the overall κ_{OA} characterization of entire organic aerosol population, and rarely specific to secondary organic aerosol factors (Kuang et al., 2020c). Considering the estimated O/C ratios of 1.17 and 0.7 for MOOA and LOOA, the retrieved κ_{LOOA} and κ_{MOOA} values are consistent with previous findings that organic aerosol oxidation state impacts significantly on organic aerosol hygroscopicity and usually higher hygroscopicity of more oxygenated organic aerosol (Kuang et al., 2020c). Especially, Lambe et al. (2011) investigated the relationships between organic aerosol hygroscopicity of laboratory generated SOA of varying kinds of volatile organic compounds using cloud condensation nuclei activity measurements and reported a linear relationship of $\kappa_{OA} = (0.18 \pm 0.04) \times O/C + 0.03$, yielding κ_{OA} values of 0.24 and 0.16 for O/C of 1.17 and 0.7, which is slight higher but generally consistent with retrieved ones of this study. Overall, the retrieved κ_{LOOA} and κ_{MOOA} are further verified indirectly through comparison with

previous literature results, confirming the strongest water uptake abilities of MOOA among OA factors.

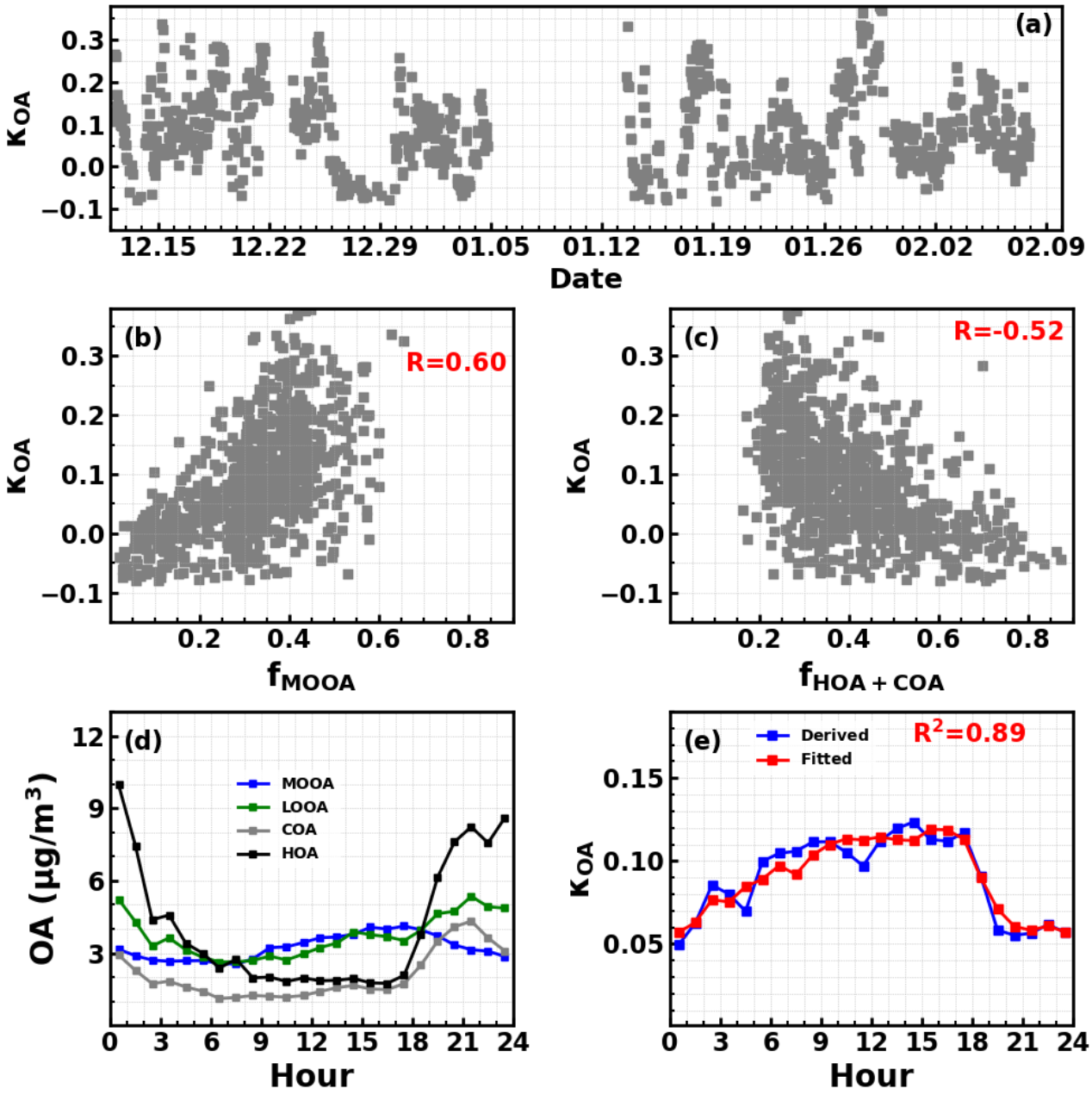

Figure 4. Timeseries of derived κ_{OA} (a); Correlations between derived κ_{OA} and mass fractions of MOOA (b), HOA+COA (c) in total organic aerosols. (d) Average diurnal variations of derived κ_{OA} (blue) and corresponding fitted ones. (e) Average diurnal variations of resolved mass concentrations of organic aerosol factors.

3.4 Dominant contribution of MOOA to organic aerosol scattering ability.

High scattering efficiency and water uptake abilities of MOOA resulted in the strongest light scattering abilities of MOOA among all organic aerosol factors. As shown in Fig.5a and Fig.5b, on average, 34% mass contribution of MOOA to entire PM_1 organic aerosol populations, however,

contributed 51% of organic aerosol scattering in dry state. The dominant role of MOOA in organic aerosol scattering would be further enhanced under ambient RH conditions due to the highest water uptake abilities of MOOA among organic aerosol factors. Results of Kuang et al. (2017) demonstrate that hygroscopicity parameter κ can be directly linked to optical hygroscopicity parameter κ_{sca} through $\kappa_{sca} = \kappa \times R_{sca}$, and thus aerosol light scattering enhancement factor f(RH). Particle number size distributions plays the most important role in R_{sca} variations with κ plays the smaller role. Yu et al. (2018) investigated R_{sca} variations from measurements of several field campaigns, found that R_{sca} varied within the range of 0.55 to 0.8 with an average of 0.66 and parameterized R_{sca} with scattering Ångström exponent. Here, the relationship between VSE_{PM1} and R_{sca} were further simulated using Mie theory through varying volume geometric mean D_{gv} of lognormal size distributions from 100 to 700 nm considering that aerosol size distributions also play the dominant role in VSE_{PM1} variations. Simulated results are shown in Fig.S11, demonstrating that R_{sca} decreased almost linearly with the increase of VSE_{PM1} for VSE_{PM1}< ~6 $m^2/\mu m^3$, however, varied complexly with VSE_{PM1} for VSE_{PM1}>~6 $m^2/\mu m^3$. According to estimated MSE_{PM1} values of LOOA, MOOA, AS, AN in Sect 4.2 and their densities introduced in Sect.2.4. VSE_{PM1} values of LOOA, MOOA, AS and AN are 4.08, 9.6, 6.9 and 8.7 $m^2/\mu m^3$, respectively. Accordingly, the $R_{sca,LOOA}$ was estimated as 0.87, and 0.63 as an average estimate was used for $R_{sca,MOOA}$, $R_{sca,AS}$ and $R_{sca,AN}$. MSEs of LOOA, MOOA, AS and AN with their water uptake abilities considered under different RH conditions can thus be estimated using $MSE_{PM1,X}(RH) = MSE_{PM1,X,dry} \times (1 + \kappa_X \times R_{sca,X} \times \frac{RH}{100-RH})$.

The problem remain that if continuous increase of MSE as a function of ambient RH increasing can be applied, because aerosol phase states were also crucial in determining the responses of aerosol scattering to RH increases (Kuang et al., 2016). Many factors such as ambient RH (Liu et al., 2017b;Liu et al., 2016), RH history aerosol particles have been experienced (Kuang et al., 2016), deliquescent and crystalline properties determined by aerosol chemical compositions and mixing states are important in determining aerosol phase state (Li et al., 2021). The ambient RH ranged from 20 to 94 with an average of 57%, with the histogram of ambient RH also shown in Fig.S12. Results of Liu et al. (2017b) found a transition from semisolid to liquid state at RH of about 60%, suggesting ambient aerosol particle might exist as semisolid or solid phase at low RH conditions. The phase state of ambient aerosols depends not only on ambient RH but also the RH history that aerosols have

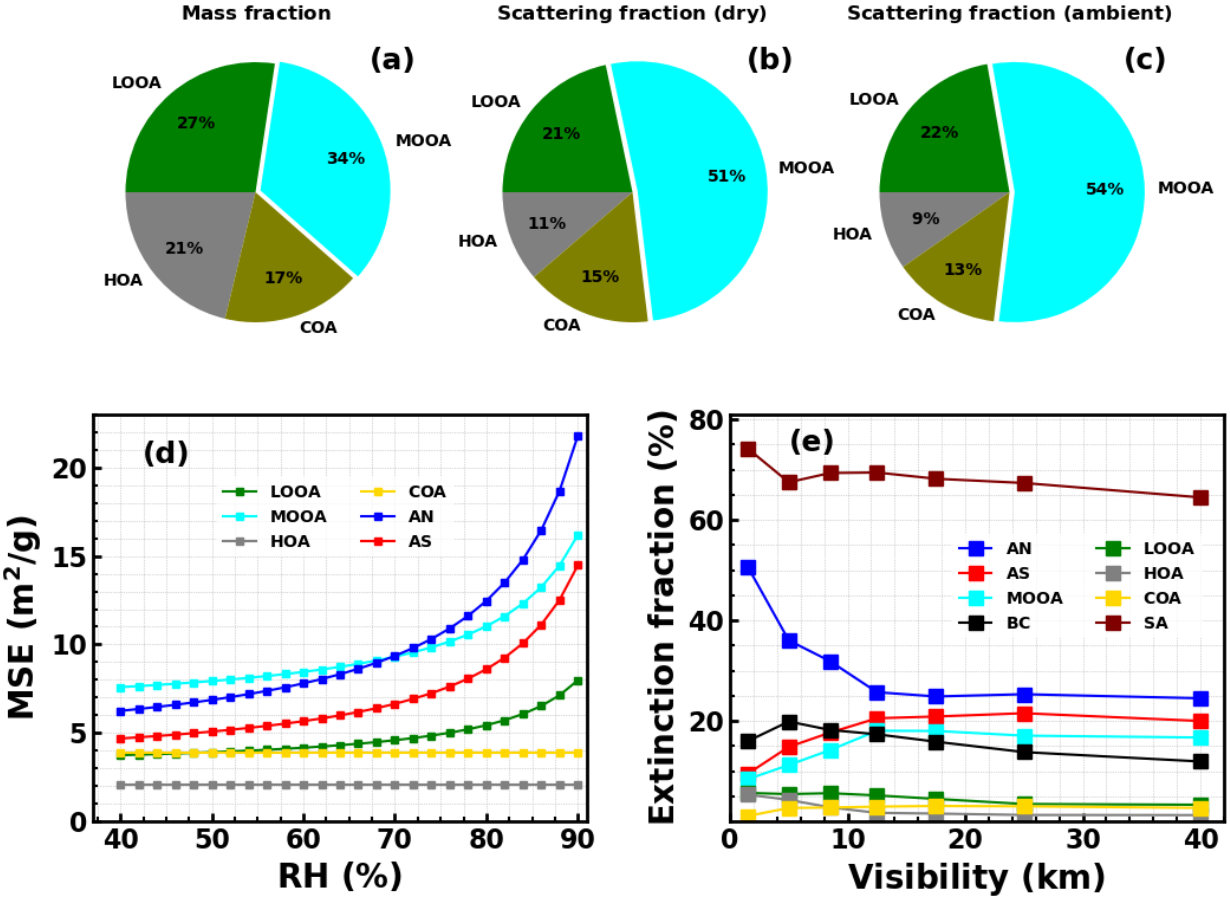

Figure 5. (a) Average mass fractions of organic aerosol components in total organic aerosol; Contributions of different organic aerosol components to total organic aerosol scattering coefficients under dry (b) and ambient (c) conditions for PM_1. (d) MSEs of aerosol components under different RH conditions. (e) Contributions of different aerosol components to visibility degradation under different visibility conditions, SA corresponds to summation of secondary aerosol components.

experienced (Kuang et al., 2016). For instance, aerosols under ambient RH of 40% in the afternoon would remain liquid if their crystalline RH is lower than 40% and they experienced high RH conditions (such as >80%) during the morning. Therefore, the lowest RH that aerosols have experienced in the afternoon and highest RH they have experienced in the morning are crucial for their phase state for hydrophilic aerosols. Besides, the deliquescent RH and crystalline RH are another two crucial parameters, however, quite complex for ambient multicomponent aerosols (Kuang et al., 2016;Li et al., 2021). Scanning RH of 60-90% was set-up for the humidified nephelometer system from 13th to 26th January and continuous increase of aerosol light scattering enhancement factor were always observed (Fig.S13) with the RH in the dry nephelometer are always lower than 35% (Fig.1a), suggesting that aerosols were either not crystalized under RH of <35% or were deliquesced under RH

of < 60%. The lines of 35% and 60% are plotted in Fig.1a and most of days (>85%) were either with its lowest RH >35% or with its highest RH>60%, suggesting liquid state in most times for internally mixed ambient secondary aerosols, and continuous increase of aerosol light scattering as ambient RH changes.

Therefore, continuous increases of MSEs of LOOA, MOOA, AN and AS as a function of RH were considered, and results are shown in Fig.5d. MSE_{PM1} of MOOA changed from 6.9 m^2/g under dry conditions to 11 and 16 m^2/g (corresponding to f(RH) values of 1.6 and 2.3) under RH of 80% and 90%, revealing that scattering abilities of MOOA would be largely enhanced by aerosol hygroscopic growth. The MSE_{PM1} of LOOA was enhanced from 3.4 under dry condition to 7 m^2/g of 90% RH, however, MSE_{PM1} values of HOA and COA remained constant due to their hydrophobic properties. Both MSE_{PM1} values of AS and AN increased quickly as a function of RH, and their f(RH) values reached as high as 2.5 and 2.2 at RH of 80%. The MSE_{PM1} of AN exceeded that of MOOA at RH near 70%, however, MSE_{PM1} of MOOA was always higher than that of AS for RH<90%. Average MSE_{PM1} values of secondary aerosol components considering water uptake under ambient RH conditions during the observation period are 6.8, 8.5, 8.9 and 4.2 m^2/g for AS, AN, MOOA and LOOA, respectively. Demonstrating strongest scattering abilities of MOOA under ambient air conditions during the observation period. Thus, the average contribution of MOOA to PM_1 organic aerosol scattering are further enhanced to 54% under ambient conditions as shown in Fig.5c (campaign average RH ~57%).

4. Implications for visibility improvement and aerosol radiative effects simulations.

Atmospheric visibility measures the maxima distance that people can see, which is determined by air extinction. The strong light scattering abilities of MOOA might have significant effects on atmospheric visibility and direct aerosol radiative effects, thus have broad implications for both aerosol environmental and climate effects. The contributions of different aerosol components to visibility degradation under different visibility conditions were estimated as fractional contributions to ambient atmospheric extinction caused by both aerosols and air molecules. The results are shown in Fig.5e, and detailed estimation method is introduced in Sect.S6 of the supplement. It shows that AN contributed most to visibility degradation especially under polluted conditions, which is consistent with findings of several recent studies that nitrate plays increasing and event dominant role in visibility degradation

(Liu et al., 2020;Li et al., 2022) in several regions of China. MOOA contributed slightly smaller than ammonium sulfate and their contributions have increased to ~20% for visibility ranges of 10-20 km. Contribution of MOOA to total organic aerosol scattering under ambient conditions was slightly higher than that under dry conditions due to the relatively low RH conditions during winter. However, the contributions of MOOA might be much higher during other seasons due to much higher RH conditions, for example, yearly average RH of >70% in Guangzhou (Xu et al., 2020). Overall, secondary aerosols contributed dominantly to visibility degradation (~70% on average), and MOOA represented the third contributor among secondary aerosol components (16% on average), demonstrating significant impacts of MOOA to visibility degradations. Thus, more attentions should be paid to property changes of SOA regarding visibility improvement investigations and policy making. Moreover, MOOA with high scattering abilities would likely contribute substantially to aerosol optical depth, and the accurate estimations of organic aerosol radiative effects in models need accurate representations of MOOA even its mass contribution to organic aerosol is small. However, constant scattering efficiency for organic aerosols derived from fixed size distributions and refractive index were usually assumed in current chemical models (Latimer and Martin, 2019) and unsatisfactory performance of current models in SOA simulations were generally reported, which hinders the accurate representations of direct aerosol radiative effects.

The role of MOOA would be likely getting more important in future due to stringent control policy of precursors of inorganic aerosol components such as sulfur dioxide and nitrogen oxides. Both formation pathways and precursor sources of MOOA are complex, however, current understandings about physical and chemical properties as well as formation pathways of MOOA remain limited. Therefore, call for more comprehensive studies on formation, evolution, and physical properties of MOOA, to better parameterize optical properties of MOOA in models and implement targeted control strategies on MOOA precursors of volatile organic compounds in the future.

Supporting information

Supporting information on site information, Q-ACSM PMF analysis, traditional multiple linear regression model analysis and visibility contribution estimation method, including 2 supporting tables and 13 supporting figures.

Competing interests. The authors declare that they have no conflict of interest.

Author Contributions. YK and LL designed the aerosol experiments. YK conceived and led this research. LL and YK wrote the manuscript. MMZ and LL conducted the Q-ACSM measurements. MMZ and YH performed the PMF analysis. BX and YK performed the humidified nephelometer system measurements. All other coauthors have contributed to this paper in different ways.

Acknowledgments

This work is supported by the National Key Research and Development Program of China (2019YFCO214605 and 2016YFC0202000); National Natural Science Foundation of China (41805109 and 42105092); Guangdong Basic and Applied Basic Research Foundation (2019A1515110791) ; Science and Technology Innovation Team Plan of Guangdong Meteorological Bureau (GRMCTD202003); Science and Technology Research Project of Guangdong Meteorological Bureau (GRMC2018M07) and Natural Science Foundation of Fujian Province, China (2021J01463).

Data availability. The data used in this study are available from the first author and corresponding author upon request.

Li Liu (liul@gd121.cn) and Ye Kuang (kuangye@jnu.edu.cn)

References

Brock, C. A., Wagner, N. L., Anderson, B. E., Attwood, A. R., Beyersdorf, A., Campuzano-Jost, P., Carlton, A. G., Day, D. A., Diskin, G. S., Gordon, T. D., Jimenez, J. L., Lack, D. A., Liao, J., Markovic, M. Z., Middlebrook, A. M., Ng, N. L., Perring, A. E., Richardson, M. S., Schwarz, J. P., Washenfelder, R. A., Welti, A., Xu, L., Ziemba, L. D., and Murphy, D. M.: Aerosol optical properties in the southeastern United States in summer – Part 1: Hygroscopic growth, Atmospheric Chemistry and Physics, 16, 4987-5007, 10.5194/acp-16-4987-2016, 2016.

Cai, J., Chu, B., Yao, L., Yan, C., Heikkinen, L. M., Zheng, F., Li, C., Fan, X., Zhang, S., Yang, D., Wang, Y., Kokkonen, T. V., Chan, T., Zhou, Y., Dada, L., Liu, Y., He, H., Paasonen, P., Kujansuu, J. T., Petäjä, T., Mohr, C., Kangasluoma, J., Bianchi, F., Sun, Y., Croteau, P. L., Worsnop, D. R., Kerminen, V.-M., Du, W., Kulmala, M., and Daellenbach, K. R.: Size-segregated particle number and mass concentrations from different emission sources in urban Beijing, Atmospheric Chemistry and Physics, 20, 12721-12740, 10.5194/acp-20-12721-2020, 2020.

Canonaco, F., Crippa, M., Slowik, J. G., Baltensperger, U., and Prévôt, A. S. H.: SoFi, an IGOR-based interface for the efficient use of the generalized multilinear engine (ME-2) for the source apportionment: ME-2 application to aerosol mass

spectrometer data, Atmos. Meas. Tech., 6, 3649-3661, 10.5194/amt-6-3649-2013, 2013.

Canonaco, F., Tobler, A., Chen, G., Sosedova, Y., Slowik, J. G., Bozzetti, C., Daellenbach, K. R., El Haddad, I., Crippa, M., Huang, R. J., Furger, M., Baltensperger, U., and Prévôt, A. S. H.: A new method for long-term source apportionment with time-dependent factor profiles and uncertainty assessment using SoFi Pro: application to 1 year of organic aerosol data, Atmos. Meas. Tech., 14, 923-943, 10.5194/amt-14-923-2021, 2021.

Chan, Y. C., Simpson, R. W., McTainsh, G. H., Vowles, P. D., Cohen, D. D., and Bailey, G. M.: Source apportionment of visibility degradation problems in Brisbane (Australia) using the multiple linear regression techniques, Atmospheric Environment, 33, 3237-3250, https://doi.org/10.1016/S1352-2310(99)00091-6, 1999.

Chen, C., Tan, H., Hong, Y., Yin, C., Deng, X., Chen, B., Wu, M., Bu, Q., Weng, J., and Gan, Q.: Characteristics, formation mechanisms, and sources of non-refractory submicron aerosols in Guangzhou, China, Atmospheric Environment, 118255, https://doi.org/10.1016/j.atmosenv.2021.118255, 2021a.

Chen, D., Zhao, Y., Zhang, J., Yu, H., and Yu, X.: Characterization and source apportionment of aerosol light scattering in a typical polluted city in the Yangtze River Delta, China, Atmos. Chem. Phys., 20, 10193-10210, 10.5194/acp-20-10193-2020, 2020.

Chen, W., Ye, Y., Hu, W., Zhou, H., Pan, T., Wang, Y., Song, W., Song, Q., Ye, C., Wang, C., Wang, B., Huang, S., Yuan, B., Zhu, M., Lian, X., Zhang, G., Bi, X., Jiang, F., Liu, J., Canonaco, F., Prevot, A. S. H., Shao, M., and Wang, X.: Real-Time Characterization of Aerosol Compositions, Sources, and Aging Processes in Guangzhou During PRIDE-GBA 2018 Campaign, Journal of Geophysical Research: Atmospheres, 126, e2021JD035114, https://doi.org/10.1029/2021JD035114, 2021b.

Cheng, Y., Zheng, G., Wei, C., Mu, Q., Zheng, B., Wang, Z., Gao, M., Zhang, Q., He, K., Carmichael, G., Pöschl, U., and Su, H.: Reactive nitrogen chemistry in aerosol water as a source of sulfate during haze events in China, Science Advances, 2, 10.1126/sciadv.1601530, 2016.

Drinovec, L., Močnik, G., Zotter, P., Prévôt, A. S. H., Ruckstuhl, C., Coz, E., Rupakheti, M., Sciare, J., Müller, T., Wiedensohler, A., and Hansen, A. D. A.: The "dual-spot" Aethalometer: an improved measurement of aerosol black carbon with real-time loading compensation, Atmospheric Measurement Techniques, 8, 1965-1979, 10.5194/amt-8-1965-2015, 2015.

Guo, J., Zhou, S., Cai, M., Zhao, J., Song, W., Zhao, W., Hu, W., Sun, Y., He, Y., Yang, C., Xu, X., Zhang, Z., Cheng, P., Fan, Q., Hang, J., Fan, S., Wang, X., and Wang, X.: Characterization of submicron particles by time-of-flight aerosol chemical speciation monitor (ToF-ACSM) during wintertime: aerosol composition, sources, and chemical processes in Guangzhou, China, Atmospheric Chemistry and Physics, 20, 7595-7615, 10.5194/acp-20-7595-2020, 2020.

Gysel, M., Crosier, J., Topping, D. O., Whitehead, J. D., Bower, K. N., Cubison, M. J., Williams, P. I., Flynn, M. J., McFiggans, G. B., and Coe, H.: Closure study between chemical composition and hygroscopic growth of aerosol particles during TORCH2, Atmos. Chem. Phys., 7, 6131-6144, 10.5194/acp-7-6131-2007, 2007.

Han, T., Xu, W., Chen, C., Liu, X., Wang, Q., Li, J., Zhao, X., Du, W., Wang, Z., and Sun, Y.: Chemical apportionment of aerosol optical properties during the Asia-Pacific Economic Cooperation summit in Beijing, China, Journal of Geophysical Research: Atmospheres, 120, 12,281-212,295, https://doi.org/10.1002/2015JD023918, 2015.

Hand, J. L., and Malm, W. C.: Review of aerosol mass scattering efficiencies from ground-based measurements since 1990, Journal of Geophysical Research: Atmospheres, 112, https://doi.org/10.1029/2007JD008484, 2007.

Hu, S., Zhao, G., Tan, T., Li, C., Zong, T., Xu, N., Zhu, W., and Hu, M.: Current challenges of improving visibility due to increasing nitrate fraction in PM2.5 during the haze days in Beijing, China, Environmental Pollution, 290, 118032, https://doi.org/10.1016/j.envpol.2021.118032, 2021.

Huang, R.-J., Zhang, Y., Bozzetti, C., Ho, K.-F., Cao, J.-J., Han, Y., Daellenbach, K. R., Slowik, J. G., Platt, S. M., Canonaco, F., Zotter, P., Wolf, R., Pieber, S. M., Bruns, E. A., Crippa, M., Ciarelli, G., Piazzalunga, A., Schwikowski, M., Abbaszade, G., Schnelle-Kreis, J., Zimmermann, R., An, Z., Szidat, S., Baltensperger, U., Haddad, I. E., and Prévôt, A. S. H.: High secondary aerosol contribution to particulate pollution during haze events in China, Nature, 514, 218, 10.1038/nature13774 https://www.nature.com/articles/nature13774#supplementary-information, 2014.

Huang, X., Ding, A., Gao, J., Zheng, B., Zhou, D., Qi, X., Tang, R., Wang, J., Ren, C., Nie, W., Chi, X., Xu, Z., Chen, L., Li, Y., Che, F., Pang, N., Wang, H., Tong, D., Qin, W., Cheng, W., Liu, W., Fu, Q., Liu, B., Chai, F., Davis, S. J., Zhang, Q., and He, K.: Enhanced secondary pollution offset reduction of primary emissions during COVID-19 lockdown in China, National Science Review, 10.1093/nsr/nwaa137, 2020.

Jimenez, J. L., Canagaratna, M. R., Donahue, N. M., Prevot, A. S. H., Zhang, Q., Kroll, J. H., DeCarlo, P. F., Allan, J. D., Coe, H., Ng, N. L., Aiken, A. C., Docherty, K. S., Ulbrich, I. M., Grieshop, A. P., Robinson, A. L., Duplissy, J., Smith, J. D., Wilson, K. R., Lanz, V. A., Hueglin, C., Sun, Y. L., Tian, J., Laaksonen, A., Raatikainen, T., Rautiainen, J., Vaattovaara, P., Ehn, M., Kulmala, M., Tomlinson, J. M., Collins, D. R., Cubison, M. J., Dunlea, J., Huffman, J. A., Onasch, T. B., Alfarra, M. R., Williams, P. I., Bower, K., Kondo, Y., Schneider, J., Drewnick, F., Borrmann, S., Weimer, S., Demerjian, K., Salcedo, D., Cottrell, L., Griffin, R., Takami, A., Miyoshi, T., Hatakeyama, S., Shimono, A., Sun, J. Y., Zhang, Y. M., Dzepina, K., Kimmel, J. R., Sueper, D., Jayne, J. T., Herndon, S. C., Trimborn, A. M., Williams, L. R., Wood, E. C., Middlebrook, A. M., Kolb, C. E., Baltensperger, U., and Worsnop, D. R.: Evolution of Organic Aerosols in the Atmosphere, Science, 326, 1525-1529, 10.1126/science.1180353, 2009.

Kuang, Y., Zhao, C. S., Ma, N., Liu, H. J., Bian, Y. X., Tao, J. C., and Hu, M.: Deliquescent phenomena of ambient aerosols on the North China Plain, Geophysical Research Letters, 43, 8744-8750, 10.1002/2016gl070273, 2016.

Kuang, Y., Zhao, C., Tao, J., Bian, Y., Ma, N., and Zhao, G.: A novel method for deriving the aerosol hygroscopicity parameter based only on measurements from a humidified nephelometer system, Atmos. Chem. Phys., 17, 6651-6662, 10.5194/acp-17-6651-2017, 2017.

Kuang, Y., Zhao, C. S., Zhao, G., Tao, J. C., Xu, W., Ma, N., and Bian, Y. X.: A novel method for calculating ambient aerosol liquid water content based on measurements of a humidified nephelometer system, Atmospheric Measurement Techniques, 11, 2967-2982, 10.5194/amt-11-2967-2018, 2018.

Kuang, Y., He, Y., Xu, W., Sun, Y., Zhao, P., Cheng, Y., Zhao, G., Tao, J., Ma, N., Su, H., Zhang, Y., Sun, J., Cheng, P., Yang, W., Zhang, S., Wu, C., and Zhao, C.: Distinct diurnal variation of organic aerosol hygroscopicity and its relationship with oxygenated organic aerosol, Atmos. Chem. Phys. Discuss., 2019, 1-33, 10.5194/acp-2019-633, 2019.

Kuang, Y., He, Y., Xu, W., Yuan, B., Zhang, G., Ma, Z., Wu, C., Wang, C., Wang, S., Zhang, S., Tao, J., Ma, N., Su, H., Cheng, Y., Shao, M., and Sun, Y.: Photochemical Aqueous-Phase Reactions Induce Rapid Daytime Formation of Oxygenated Organic Aerosol on the North China Plain, Environmental science & technology, 10.1021/acs.est.9b06836, 2020a.

Kuang, Y., He, Y., Xu, W., Zhao, P., Cheng, Y., Zhao, G., Tao, J., Ma, N., Su, H., Zhang, Y., Sun, J., Cheng, P., Yang, W., Zhang, S., Wu, C., Sun, Y., and Zhao, C.: Distinct diurnal variation in organic aerosol hygroscopicity and its relationship with oxygenated organic aerosol, Atmos. Chem. Phys., 20, 865-880, 10.5194/acp-20-865-2020, 2020b.

Kuang, Y., Xu, W., Tao, J., Ma, N., Zhao, C., and Shao, M.: A Review on Laboratory Studies and Field Measurements of Atmospheric Organic Aerosol Hygroscopicity and Its Parameterization Based on Oxidation Levels, Current Pollution Reports, 10.1007/s40726-020-00164-2, 2020c.

Kuang, Y., Huang, S., Xue, B., Luo, B., Song, Q., Chen, W., Hu, W., Li, W., Zhao, P., Cai, M., Peng, Y., Qi, J., Li, T., Chen, D., Yue, D., Yuan, B., and Shao, M.: Contrasting effects of secondary organic aerosol formations on organic aerosol hygroscopicity, Atmos. Chem. Phys. Discuss., 2021, 1-27, 10.5194/acp-2021-3, 2021a.

Kuang, Y., Huang, S., Xue, B., Luo, B., Song, Q., Chen, W., Hu, W., Li, W., Zhao, P., Cai, M., Peng, Y., Qi, J., Li, T., Wang, S., Chen, D., Yue, D., Yuan, B., and Shao, M.: Contrasting effects of secondary organic aerosol formations on organic aerosol hygroscopicity, Atmos. Chem. Phys., 21, 10375-10391, 10.5194/acp-21-10375-2021, 2021b.

Kuwata, M., Zorn, S. R., and Martin, S. T.: Using Elemental Ratios to Predict the Density of Organic Material Composed of Carbon, Hydrogen, and Oxygen, Environmental science & technology, 46, 787-794, 10.1021/es202525q, 2012.

Lambe, A. T., Onasch, T. B., Massoli, P., Croasdale, D. R., Wright, J. P., Ahern, A. T., Williams, L. R., Worsnop, D. R., Brune, W. H., and Davidovits, P.: Laboratory studies of the chemical composition and cloud condensation nuclei (CCN) activity of secondary organic aerosol (SOA) and oxidized primary organic aerosol (OPOA), Atmos. Chem. Phys., 11, 8913-8928,

10.5194/acp-11-8913-2011, 2011.
Latimer, R. N. C., and Martin, R. V.: Interpretation of measured aerosol mass scattering efficiency over North America using a chemical transport model, Atmos. Chem. Phys., 19, 2635-2653, 10.5194/acp-19-2635-2019, 2019.
Li, K., Li, J., Liggio, J., Wang, W., Ge, M., Liu, Q., Guo, Y., Tong, S., Li, J., Peng, C., Jing, B., Wang, D., and Fu, P.: Enhanced Light Scattering of Secondary Organic Aerosols by Multiphase Reactions, Environmental science & technology, 51, 1285-1292, 10.1021/acs.est.6b03229, 2017.
Li, W., Teng, X., Chen, X., Liu, L., Xu, L., Zhang, J., Wang, Y., Zhang, Y., and Shi, Z.: Organic Coating Reduces Hygroscopic Growth of Phase-Separated Aerosol Particles, Environmental science & technology, 55, 16339-16346, 10.1021/acs.est.1c05901, 2021.
Li, Z., Sun, Y., Wang, Q., Xin, J., Sun, J., Lei, L., Li, J., Fu, P., and Wang, Z.: Nitrate and secondary organic aerosol dominated particle light extinction in Beijing due to clean air action, Atmospheric Environment, 269, 118833, https://doi.org/10.1016/j.atmosenv.2021.118833, 2022.
Liu, H. J., Zhao, C. S., Nekat, B., Ma, N., Wiedensohler, A., van Pinxteren, D., Spindler, G., Müller, K., and Herrmann, H.: Aerosol hygroscopicity derived from size-segregated chemical composition and its parameterization in the North China Plain, Atmos. Chem. Phys., 14, 2525-2539, 10.5194/acp-14-2525-2014, 2014.
Liu, J., Ren, C., Huang, X., Nie, W., Wang, J., Sun, P., Chi, X., and Ding, A.: Increased Aerosol Extinction Efficiency Hinders Visibility Improvement in Eastern China, Geophysical Research Letters, 47, e2020GL090167, https://doi.org/10.1029/2020GL090167, 2020.
Liu, M., Bi, J., and Ma, Z.: Visibility-Based PM2.5 Concentrations in China: 1957-1964 and 1973-2014, Environmental science & technology, 51, 13161-13169, 10.1021/acs.est.7b03468, 2017a.
Liu, P., Zhang, Y., and Martin, S. T.: Complex Refractive Indices of Thin Films of Secondary Organic Materials by Spectroscopic Ellipsometry from 220 to 1200 nm, Environmental science & technology, 47, 13594-13601, 10.1021/es403411e, 2013.
Liu, P., Li, Y. J., Wang, Y., Gilles, M. K., Zaveri, R. A., Bertram, A. K., and Martin, S. T.: Lability of secondary organic particulate matter, Proceedings of the National Academy of Sciences, 201603138, 10.1073/pnas.1603138113, 2016.
Liu, Y., Wu, Z., Wang, Y., Xiao, Y., Gu, F., Zheng, J., Tan, T., Shang, D., Wu, Y., Zeng, L., Hu, M., Bateman, A. P., and Martin, S. T.: Submicrometer Particles Are in the Liquid State during Heavy Haze Episodes in the Urban Atmosphere of Beijing, China, Environmental Science & Technology Letters, 4, 427-432, 10.1021/acs.estlett.7b00352, 2017b.
Ng, N. L., Herndon, S. C., Trimborn, A., Canagaratna, M. R., Croteau, P. L., Onasch, T. B., Sueper, D., Worsnop, D. R., Zhang, Q., Sun, Y. L., and Jayne, J. T.: An Aerosol Chemical Speciation Monitor (ACSM) for Routine Monitoring of the Composition and Mass Concentrations of Ambient Aerosol, Aerosol Science and Technology, 45, 780-794, 10.1080/02786826.2011.560211, 2011.
Qiu, J., Tan, W., Zhao, G., Yu, Y., and Zhao, C.: New correction method for the scattering coefficient measurements of a three-wavelength nephelometer, Atmos. Meas. Tech., 14, 4879-4891, 10.5194/amt-14-4879-2021, 2021.
Sun, Y. L., Wang, Z. F., Fu, P. Q., Yang, T., Jiang, Q., Dong, H. B., Li, J., and Jia, J. J.: Aerosol composition, sources and processes during wintertime in Beijing, China, Atmos. Chem. Phys., 13, 4577-4592, 10.5194/acp-13-4577-2013, 2013.
Tao, J., Zhang, Z., Wu, Y., Zhang, L., Wu, Z., Cheng, P., Li, M., Chen, L., Zhang, R., and Cao, J.: Impact of particle number and mass size distributions of major chemical components on particle mass scattering efficiency in urban Guangzhou in southern China, Atmos. Chem. Phys., 19, 8471-8490, 10.5194/acp-19-8471-2019, 2019.
Titos, G., Cazorla, A., Zieger, P., Andrews, E., Lyamani, H., Granados-Muñoz, M. J., Olmo, F. J., and Alados-Arboledas, L.: Effect of hygroscopic growth on the aerosol light-scattering coefficient: A review of measurements, techniques and error sources, Atmospheric Environment, 141, 494-507, https://doi.org/10.1016/j.atmosenv.2016.07.021, 2016.
Wang, J., Ye, J., Zhang, Q., Zhao, J., Wu, Y., Li, J., Liu, D., Li, W., Zhang, Y., Wu, C., Xie, C., Qin, Y., Lei, Y., Huang, X., Guo, J., Liu, P., Fu, P., Li, Y., Lee, H. C., Choi, H., Zhang, J., Liao, H., Chen, M., Sun, Y., Ge, X., Martin, S. T., and Jacob, D. J.: Aqueous

production of secondary organic aerosol from fossil-fuel emissions in winter Beijing haze, Proceedings of the National Academy of Sciences, 118, e2022179118, 10.1073/pnas.2022179118, 2021.

Wang, Y., Chen, J., Wang, Q., Qin, Q., Ye, J., Han, Y., Li, L., Zhen, W., Zhi, Q., Zhang, Y., and Cao, J.: Increased secondary aerosol contribution and possible processing on polluted winter days in China, Environment International, 127, 78-84, https://doi.org/10.1016/j.envint.2019.03.021, 2019.

Wu, Z. J., Zheng, J., Shang, D. J., Du, Z. F., Wu, Y. S., Zeng, L. M., Wiedensohler, A., and Hu, M.: Particle hygroscopicity and its link to chemical composition in the urban atmosphere of Beijing, China, during summertime, Atmos. Chem. Phys., 16, 1123-1138, 10.5194/acp-16-1123-2016, 2016.

Xu, W., Sun, Y., Wang, Q., Zhao, J., Wang, J., Ge, X., Xie, C., Zhou, W., Du, W., Li, J., Fu, P., Wang, Z., Worsnop, D. R., and Coe, H.: Changes in Aerosol Chemistry From 2014 to 2016 in Winter in Beijing: Insights From High-Resolution Aerosol Mass Spectrometry, Journal of Geophysical Research: Atmospheres, 124, 1132-1147, 10.1029/2018jd029245, 2019.

Xu, W., Kuang, Y., Bian, Y., Liu, L., Li, F., Wang, Y., Xue, B., Luo, B., Huang, S., Yuan, B., Zhao, P., and Shao, M.: Current Challenges in Visibility Improvement in Southern China, Environmental Science & Technology Letters, 7, 395-401, 10.1021/acs.estlett.0c00274, 2020.

Yu, Y., Zhao, C., Kuang, Y., Tao, J., Zhao, G., Shen, C., and Xu, W.: A parameterization for the light scattering enhancement factor with aerosol chemical compositions, Atmospheric Environment, 191, 370-377, https://doi.org/10.1016/j.atmosenv.2018.08.016, 2018.

Zhao, C., Yu, Y., Kuang, Y., Tao, J., and Zhao, G.: Recent Progress of Aerosol Light-scattering Enhancement Factor Studies in China, Advances in Atmospheric Sciences, 36, 1015-1026, 10.1007/s00376-019-8248-1, 2019a.

Zhao, G., Tan, T., Zhao, W., Guo, S., Tian, P., and Zhao, C.: A new parameterization scheme for the real part of the ambient urban aerosol refractive index, Atmos. Chem. Phys., 19, 12875-12885, 10.5194/acp-19-12875-2019, 2019b.

Zhao, G., Hu, M., Fang, X., Tan, T., Xiao, Y., Du, Z., Zheng, J., Shang, D., Wu, Z., Guo, S., and Zhao, C.: Larger than expected variation range in the real part of the refractive index for ambient aerosols in China, Science of The Total Environment, 779, 146443, https://doi.org/10.1016/j.scitotenv.2021.146443, 2021.

Zhou, W., Xu, W., Kim, H., Zhang, Q., Fu, P., Worsnop, D. R., and Sun, Y.: A review of aerosol chemistry in Asia: insights from aerosol mass spectrometer measurements, Environmental Science: Processes & Impacts, 22, 1616-1653, 10.1039/D0EM00212G, 2020.